

## Corrosion Behavior of Cast Iron in the Presence of *Acidithiobacillus Ferrooxidans*

Li Lin<sup>1,2,4</sup>, Cheng Liu<sup>2,4</sup>, Lei Fu<sup>3</sup>, Ying Zeng<sup>1,\*</sup>, Min Gong<sup>2,4,\*\*</sup>, Xue jun Cui<sup>2,4</sup>, Junchen Meng<sup>2,4</sup>, Xin jie Huang<sup>3</sup>

<sup>1</sup> College of Materials and Chemistry and Chemical Engineering, Chengdu University of Technology, Chengdu 610059, China

<sup>2</sup> Key Laboratory of Material Corrosion and Protection of Sichuan Province, Zigong 643000, China

<sup>3</sup> School of Mechanical Engineering, Sichuan University of Science & Engineering, Zigong 643000, China

<sup>4</sup> School of Material Science and Engineering, Sichuan University of Science & Engineering, Zigong 643000, China

\*E-mail: [zengy@cdut.edu.cn](mailto:zengy@cdut.edu.cn)

\*\*E-mail: [gongmin@suse.edu.cn](mailto:gongmin@suse.edu.cn)

Received: 1 October 2020 / Accepted: 28 November 2020 / Published: 31 December 2020

---

*Ferrooxidans* bacteria occur widely in acid mine drainage water. This work examined the corrosion behavior of cast iron in the presence of the acidophilic iron-oxidizing bacterium *Acidithiobacillus ferrooxidans* (*T.f.*). Results showed this bacterium accelerated corrosion of cast iron by a factor of two compared with that of acidic (pH 2) water. This bacterium oxidizes ferrous ions to ferric ions as a source of energy and the produced ferric ions is quickly hydrolyzed to generate hydrogen ions, which partly offsets that consumed in the corrosion reaction. Besides, pitting was found on the cast iron surface in culture medium containing *Acidithiobacillus ferrooxidans*.

---

**Keywords:** Cast iron; MIC; Weight loss; morphology; EIS

### 1. INTRODUCTION

Iron-oxidizing bacteria (IOB) and iron-reducing bacteria (IRB) are widespread in nature. As electron donors and acceptors, respectively, IOB and IRB exerted primary controls on the redox-induced cycling of iron in the environment by using  $\text{Fe}^{2+}$  and  $\text{Fe}^{3+}$  bound in solid-phase iron minerals [1-3]. IRB were capable of completely removing previously formed rusting on the surface of carbon steel coupons using  $\text{Fe}^{3+}$  ions as electron acceptors [4]. Bioaugmentation with IRB was an effective method to enhance the activity of iron reduction [5]. In particular, *Pseudomonas* (an IOB) was found

to inhibit corrosion of Q235 carbon steel in a magnetic field [6]. The metabolic products of *Pseudomonas* and some coatings were found to have a corrosion inhibition [7-9].

*T.f* is an IOB. It is an important industrial microorganism that was first discovered by Colmer and Hinkle in 1947 in coal mine wastewater and found to promote the oxidation of pyrite in a coal mining environment [10]. *T.f* is Gram-negative. It has characteristics of chemical autotrophy, is aerobic and acidophilic and is suitable for use in a medium-temperature environment. *T.f* is able to capitalize on  $Fe^{2+}$  as an electron donor and oxidize ferrous to ferric ions, which can couple with the generation of nicotinamide dehydrogenase (NADPH) and the synthesis of adenosine triphosphate (ATP) to provide energy to cells [11]. It was shown by starvation experiments that bacteria could obtain energy by extracellular electron transfer, too [12].

The step enabled biological oxidation to proceed smoothly.

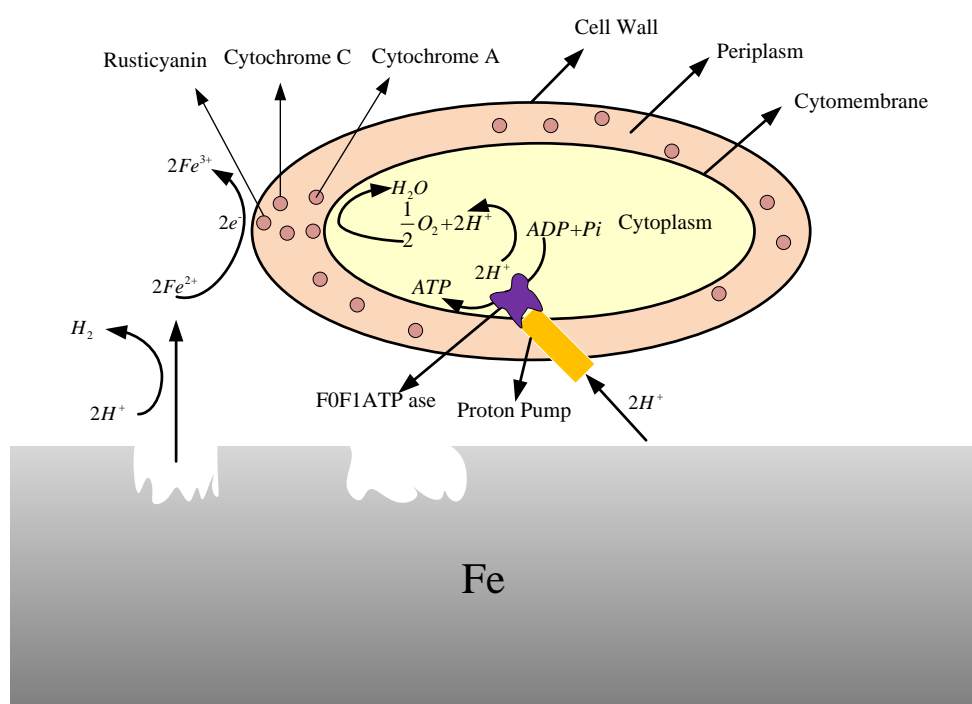


**Figure 1.** Schematic diagram of electron transfer in cells

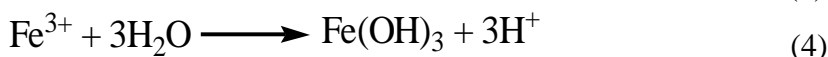
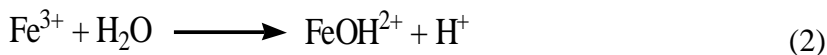
Many scholars have studied the biological oxidation of ferrous sulfate by *T.f* [13-16]. Electrons from the bacterial outer membrane are transported to cytochrome c in the periplasm through rusticyanin; the reduced cytochrome c binds to the cell membrane and then passes electrons to cytochrome a. Reduced cytochrome a then releases electrons to oxygen molecules to generate water. The possible process of electron in the biological oxidation chain is summarized as follows :



Energy is released in each step of this electron-transfer process, which provides for the growth of *T.f* and generation of NADPH (reduction of coenzyme II, which is involved in the electron-transfer chain). In this process, ferrous ions react in an acid solution containing *T.f* as follow:



the pH initially increases because ferrous oxidation is accompanied by the consumption of  $\text{H}^+$  when *T.f* is grown in ferrous sulfate solution [17]; ferric ions are hydrolyzed to produce acid, which lowers the pH.



*T.f* is widely used for desulfurization, bioleaching, and treatment of wastewater and heavy metal sludge due to its ability to oxidize ferrous ions and sulfides. Rai desulphurized coal containing 2% ~ 8% sulfur using *T.f*, and found that 80%~85% of pyritic sulfur could be effectively removed [18]. Yang et al. found that the presence of *T.f* was conducive to improving Ni yield, shortening leaching time, and reducing costs in the bioleaching of pentlandite: a Ni leaching extent of 83.8% was obtained after 5 days [19]. Torma et al. studied the bioleaching of stibnite, and the results showed that the biooxidation rate of stibnite more than doubled in the presence of *T.f* [20]. Kaewkannetra et al. investigated bioleaching of zinc from a 12% zinc-bearing gold deposit in Thailand, and showed that the leaching rate was greatly improved by the presence of this bacterium [21]. Wood et al. immobilized *T.f* on sand, designed a continuous process, and demonstrated that it worked well in the repeated treatment of acid mine-drainage [22]. Gómez et al. utilized *T.f* to extract 80% of the heavy metals (cadmium, cobalt, copper, and zinc) present in a rainwater sludge, and found that bioleaching had a certain remediation effect on heavy metal-contaminated soil [23].

*T.f* resulted in a greater dissolution of silica and a higher silicide corrosion rate [24]. The corrosion behavior of mild steel C1010 was studied in the environment containing this IOB. Results showed that *T.f* accelerated mild steel C1010 corrosion by a factor of 3–6 times that of acidic water at pH 2 [25]. Pisapia et al. found that *T.f* aggravated pitting corrosion of pyrite [26]. Corrosion pits were found on the surface after 10CrNiCu steel had been immersed in the existing *T.f* bacterial system for 21 days, whereas no pitting resulted after immersion for the same time in a sterile system [27]. Some anaerobic bacteria also caused serious corrosion of steel materials, such as sulfate-reducing bacteria (SRB) [28-31].

*T.f*, widely presented in acidic mine drainage could oxidize ferrous to ferric ion. In this study, the corrosion behavior of cast iron was studied by using different characterization methods, such as weight loss, scanning electron microscopy (SEM), open-circuit potential (OCP) and electrochemical impedance spectroscopy (EIS). Electrochemical measurements were used for the first time to investigate the corrosion of cast iron in an environment that contained *T.f*. Changes in the  $E_{cor}$  and EIS of the cast iron were obtained from electrochemical tests, and the electron transfer of cast iron was discussed. Local corrosion and crevice corrosion of cast iron was analyzed. The corrosion behavior and mechanism of microbiologically induced corrosion (MIC) was discussed in the hope that innovative pipeline materials and corrosion inhibitors could be created and the service life of iron-based equipments could be prolonged.

## 2. EXPERIMENTAL SECTION

### 2.1 Materials

Cast iron was used in the experiment, and its composition was listed in Table 1.

**Table 1.** Composition of cast iron (wt%)

elements	C	Si	Mn	P	S	Mg	Fe
content	3.6-3.9	1.8-2.4	0.25-0.4	<0.06	<0.08	0.03-0.05	balance

The material was machined into rectangle sample coupons of 50mm×25 mm×3mm and 15 mm ×10 mm×3mm with holes 5 mm and 3mm diameter, respectively. The large rectangle coupons were polished in sequence from 120#, 240#, 320#, 400#, 600#, 800# to 1000# using metallographic sandpaper, and were used for corrosion weight loss and corrosion product detection. The small coupons were polished stepwise from 120#, 240#, 320#, 400#, ...to 1200# paper, and carefully burnished for observation of surface morphology after corrosion. Circular coupons with a diameter of 11.4mm were machined, polished stepwise to a 1200# finish, and burnished to a mirror gloss for use in the electrochemical experiments. All coupons were cleaned with acetone before polishing, washed with ultra-pure water after polishing, disinfected with 75% ethanol, dehydrated with anhydrous ethanol, quickly dried with cold air, then placed in a disinfection cabinet prior to use. The samples were sterilized in UV for 20 min before each experiment.

### 2.2 Strain culture

The experimental strain of *Acidithiobacillus ferrooxidans* was isolated and purified from a mine drainage solution. It was grown in a 9K fluid nutrient media [32]. Solution A: (NH<sub>4</sub>)<sub>2</sub>SO<sub>4</sub> 3.0g, K<sub>2</sub>HPO<sub>4</sub> 0.5g, KCl 0.10g, Ca(NO<sub>3</sub>)<sub>2</sub> 0.01g, MgSO<sub>4</sub>·7H<sub>2</sub>O 0.5g, Milli-Q water 600mL. The solution was adjusted to pH 2.0 by addition of 6 mol/L H<sub>2</sub>SO<sub>4</sub>. Solution A was placed in a 1-L reagent bottle and then sterilized at 121°C and 1×10<sup>5</sup> Pa in a high-pressure sterilization pot for 20 min.

Solution B: FeSO<sub>4</sub>·7H<sub>2</sub>O 44.7 g, Milli-Q water 400 mL, which was adjusted to pH 2.0 using 6 mol/L H<sub>2</sub>SO<sub>4</sub>, followed by filtration and sterilization with a sand core filter and a circulating water vacuum pump. The filter membrane was a polyethersulfone membrane with an aperture of 0.22 μm and a diameter of 50 mm.

Solution A and B were mixed before inoculation. The mixture solution was used as culture medium. The proportion of bacterial solution that was inoculated into the bacteria system was 10%, and the control group was a sterile system. The only difference between the two groups was bacterial liquid addition or lack thereof.

The medium solution was light green initially, which was the color of Fe<sup>2+</sup>. After preculturing for 2 days at 30°C and at a shaking rate of 100 rpm/min, the solution turned reddish brown after being cultured in the *T.f* system because Fe<sup>2+</sup> could be oxidized to Fe<sup>3+</sup> by the bacteria. The liquid color

remained unchanged when it was cultivated in the sterile system. Burnished coupons were placed in the two solution systems. Each experimental group contained three large and two small coupons, which were incubated under the same conditions (30°C and 100 rpm/min).

### 2.3 Analysis of corrosion morphology

Each group of coupons was immersed in the culture medium for a predetermined time and then removed. After freeze-drying, the morphology of the coupon products was observed by SEM (VegaIII, TESCAN, CZ). The corrosion products were then thoroughly removed to observe the morphology of the corrosion pits on the sample surface.

### 2.4 Electrochemical measurement

The electrochemical tests were conducted by using a potentiostat (Solartron SI 1287+ Solartron SI 1260, AMETEK, UK). A three-electrode system was used, which consisted of a polished cast iron sample, a saturate calomel electrode (SCE) and a platinum foil as the working electrode, reference electrode and auxiliary electrode, respectively. The electrochemical experiments were controlled by using Zplot and Corrware software.

The OCP and EIS of the working electrodes immersed in the sterile and *T.f* systems were measured for different contact time. EIS was measured at the self-etching potential. The excitation signal was a 5mV sine wave and the test frequency range was 10 mHz-100 kHz. The EIS results were fitted by ZSimpWin software.

## 3. RESULTS AND DISCUSSION

### 3.1 Corrosion weight loss

The average corrosion rates of cast iron immersed in the sterile and *T.f* systems were calculated based on weight loss method after immersion for 4, 8, 12, 16, and 20 days. The sterile liquid and *T.f* medium were replaced every 4 days.

The results in Fig. 2 showed that the corrosion weight losses of *T.f* and sterile systems differed significantly: that of the *T.f* system was about twice that of the sterile system, indicating that the *T.f* strain grew steadily in the bacterial liquid and played an oxidation role. Ferrous iron was oxidized to ferric iron, and hydrogen ions were hydrolyzed by the continuous consumption of ferric iron. Ferric iron hydrolyzed easily to form hydrogen ions according to Equations (2-4). According to the principles of chemical equilibrium, ferrous iron continued to lose electrons to form ferric iron in the bacterial system, so the reaction of iron dissolution to form ferrous iron continued, resulting in increased corrosion of the cast iron coupons. Two kinds of electron transfer mediators, flavin adenine dinucleotide (FAD) and riboflavin, accelerated considerably pitting of C1018 steel in *P. aeruginosa* [33]. These results resulted from electron transfer.

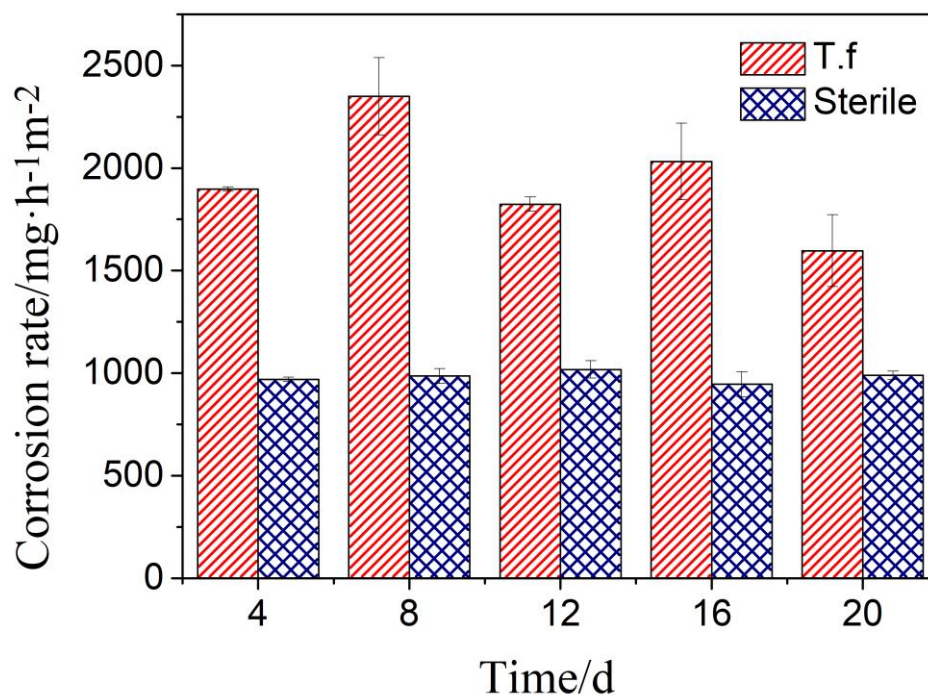
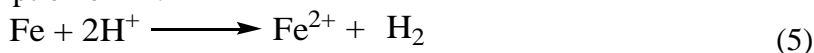


**Figure 2.** Corrosion rates of cast iron coupons exposed in *T.f* and sterile cultures for different days

### 3.2 pH value

The coupons reacted in acidic solution to yield hydrogen gas, so the pH increased owing to the consumption of  $H^+$ .



The evolution of small bubbles was observed during the experiment. Owing to the oxidation of *T.f*, ferrous iron was converted to ferric, the hydrolysis of which produced acid, which, in turn, led to continuous reaction and increasing corrosion. The reaction was presented as Equation (2-4).

The pH values of the two systems were measured during the reaction. Similarly, *Acidithiobacillus caldus SM-1* could decrease the pH under the biofilm, which lead to severe pitting against S32654 stainless steel, which was usually considered a corrosion-resistant metal [34].

**Table 2.** The pH of in *T.f* and sterile for different days

time (d)	<i>T.f</i> pH	sterile pH
0.5	2.5±0.1	3.0±0.1
1	2.7±0.1	3.5±0.1
2	3.3±0.1	3.8±0.1
4	3.5±0.1	4.0±0.1
8	3.5±0.1	4.0±0.1
12	3.5±0.1	4.0±0.1
16	3.5±0.1	4.0±0.1

Table 2 showed that the final pH of the *T.f* system was lower than that of the sterile system, indicating that the former produced acid stably during this process.

Iron was oxidized to ferrous iron, and then the ferrous was oxidized to ferric iron. In this oxidation process, *T.f* obtained energy for its growth needs, and accelerated metal corrosion. Ferric iron was subsequently hydrolyzed to release acid in aqueous solution, which partially offset the  $H^+$  consumed by corrosion of the coupons. As a result, the pH of the *T.f* system eventually reached a value of about 3.5, which was lower than that of the sterile system. Three reactions, i.e. (2), (3), and (4), were responsible for the continuation corrosion and the viability of the cells at a low pH ( $3.5 \pm 0.1$ ).

### 3.3 Surface analysis

#### 3.3.1 Corrosion film morphology

As shown in Fig. 3, after 6 h immersion, obvious corrosion product films were formed on the surfaces of the coupons in both systems.

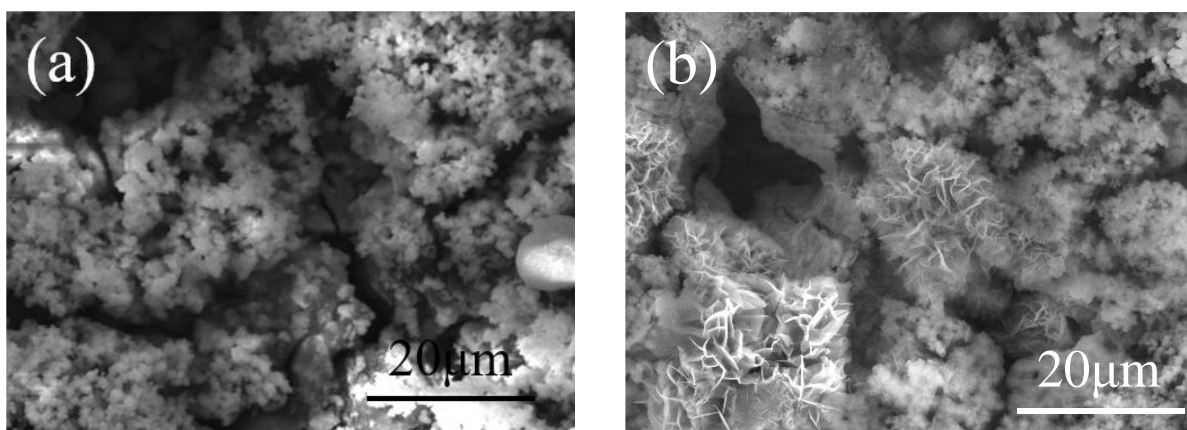
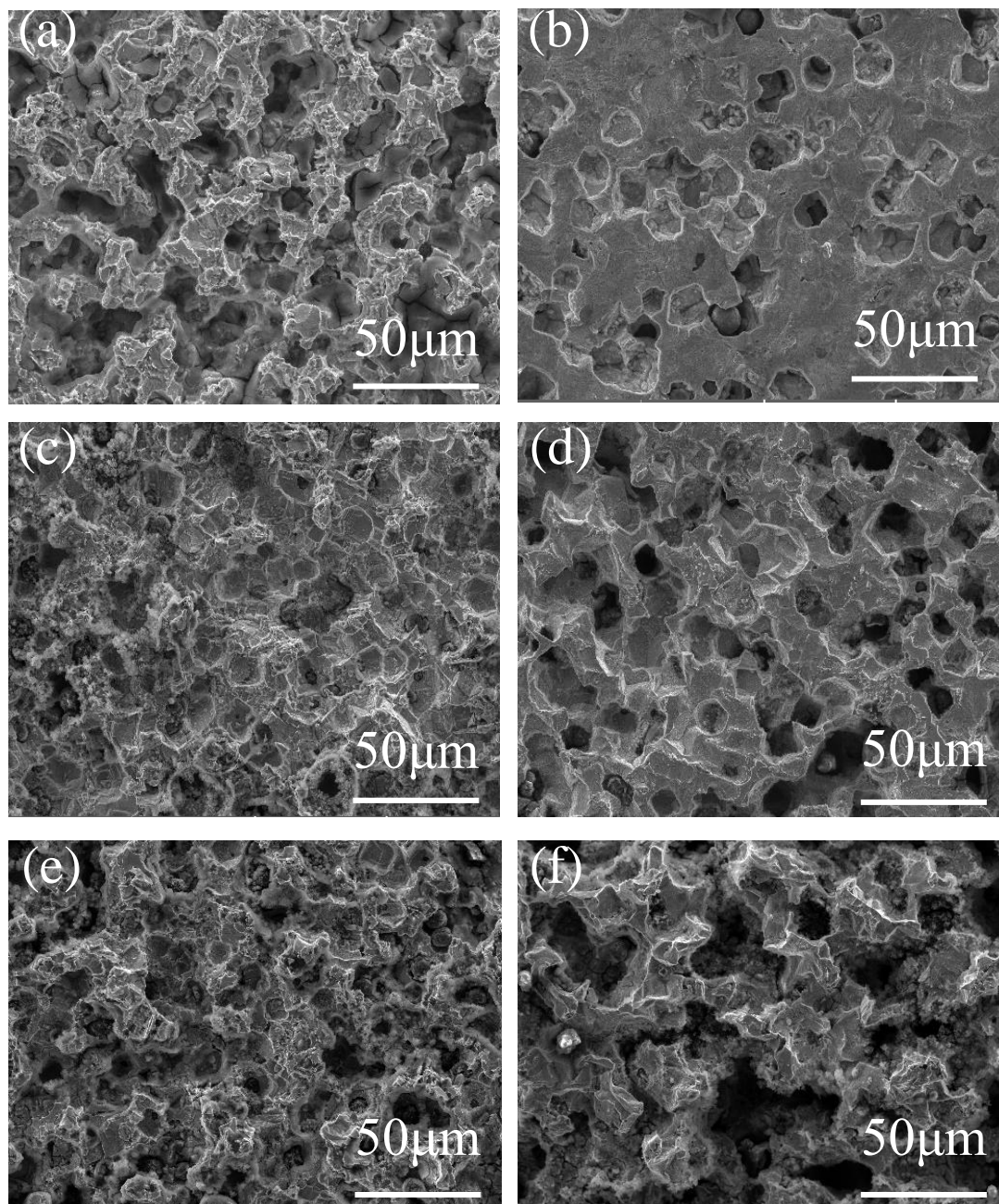


**Figure 3.** (a) The corrosion morphology of cast iron in *T.f* system for 6h (b) The corrosion morphology of cast iron in sterile system for 6h

In the *T.f* system, the corrosion products took the form of fragments in some regions and spheres in others, with cracks on the surface. This result differed from the experimental consequence where corrosion products were round, compact and loose around the center by Li [35]. This result may be ascribed to the difference in metal material. The uneven distribution of corrosion products and cracks easily created an oxygen concentration difference cell, which enabled conditions for local or crevice corrosion of the materials. In the sterile system, the corrosion products were denser and thicker, and there were lamellar products arranged in a dense and orderly manner in local areas. The relatively dense corrosion product film inhibited corrosion of cast iron to some extent.

3.3.2 Scanning electron microscopy of corrosion morphology

Fig. 4 showed SEM images of the corrosion morphologies of the coupon surfaces taken at 400 times magnification for the *T.f* and sterile system for different immersion periods.



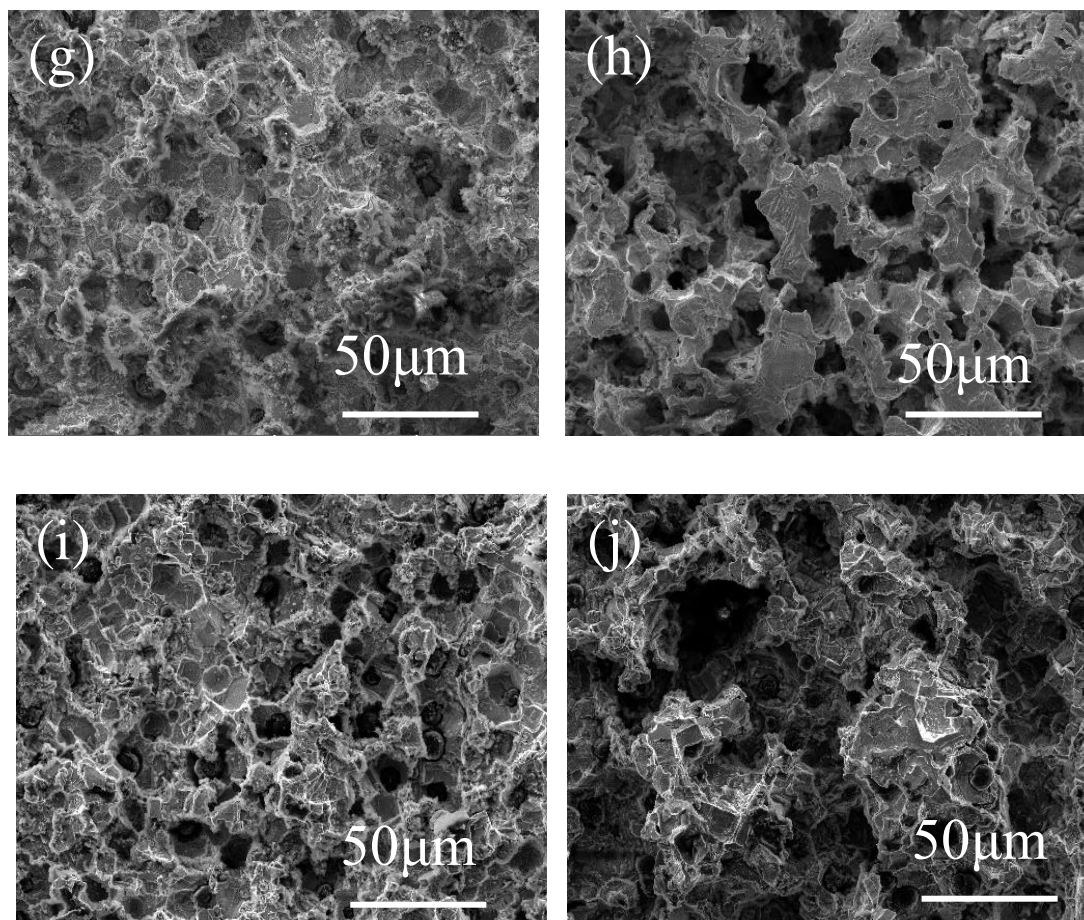


**Figure 4.** The SEM images of corrosion morphology (composite film removed) for different days, *T.f*: (a) 0.25d; (c) 0.5d; (e) 1d; (g) 2d; (i) 4d; Sterile: (b) 0.25d; (d) 0.5d; (f) 1d; (h) 2d; (j) 4d;

After immersion for 6 h, the SEM images showed that the cast iron in both systems exhibited uniform corrosion. In the *T.f* system, the surface of the iron had a greater number and deeper corrosion pits; in the sterile system, the surface was flat and the number of corrosion pits was small. In both systems, the surface morphology showed uniformly distributed corrosion pits, but their depth varied. One reason for this difference was that metal atoms in positions of dislocation outcrops, spiral dislocation step ends, and similar structures were preferentially removed from the lattice when the metal underwent anodic dissolution. Secondly, impurities in the metal gave the cast iron an uneven composition, which impacted the electrochemical performance. Preferential corrosion occurred in regions with low electrode potential, resulting in different depths of corrosion pits. Thirdly, the adsorption of bacteria was random in the *T.f* system, and corrosion was more serious in regions where there were a large number of bacteria.

After soaking for 12 h, the area of surface corrosion was larger, and the corrosion pits had become linked in the *T.f* system. This may be ascribed to the formation of a biofilm on the surface of the cast iron by *T.f* during the initial experimental period and bacteria accumulated on the surface, which accelerated the corrosion. In the sterile system, the areas and depths of corrosion pits on the

surface of cast iron were less than those in the *T.f* system, and linkages of corrosion pits did not occur on the surface.

After 1-4 d of immersion, the corrosion surface of the sample in the sterile control system was flat, but there were still corrosion pits, the depths of which were less than those of the *T.f* system. In the later stages of the experiment, the number of pits increased; these were round, deep, and concentrated. In the *T.f* system, ferrous iron was sequentially oxidized by *T.f*, which circulated and accelerated the corrosion, causing the pitting corrosion to continuously deepen until the required inorganic substances and energy were exhausted and the bacterial strain stopped growing. Pitting formation resulted from bacterial accumulation that resulted in local pH reduction and a difference in biofilm. In addition, an oxygen-concentration cell formed [35].

It could be seen from Fig. 4(i) and (j) that the corrosion pits of the coupon in sterile group seemed deeper than those in *T.f*. However, compared with the weight loss results, it could be known that the coupon in *T.f* was corroded much more seriously because the surface of the sample had been etched away and it became much thinner while only some pits appeared at the surface of the specimen in sterile group.

In summary, the corrosion in the *T.f* system intensified with increasing immersion time. The corrosion pits became linked together and their depth gradually increased. The extent of corrosion in the sterile system also increased, but not to the same extent. In short, *T.f* promoted the corrosion of cast iron. The conclusion was the same as corrosion weight loss.

### 3.4 Electrochemical test results

#### 3.4.1 Open circuit potential

In the electrochemical test process, the bacterial medium was precultured for 3 days and then transferred to a modified electrochemical test reactor that comprised a four-necked flask. Changes in the OCP of cast iron measured in the *T.f* and sterile systems with time were shown in Figs. 5(a) and (b), respectively.

The OCP of the electrode shifted in the negative direction and changed significantly when the coupons were soaked in the *T.f* system for 6-12 h. This was due to excessive bacterial growth during the initial soaking stage and incomplete biofilm formation on the cast iron surface. The matrix of the material was therefore vulnerable to the corrosion medium and the corrosion tendency of the material gradually increased. The negative shift of the OCP of the working electrode was not obvious from 12 h to 1 d because the bacteria formed a biofilm on its surface and the corrosion product was dense, which acted as a barrier. For immersion 1-5 d, the cast iron samples were continuously corroded and the OCP continued to be shifted to more negative potentials.

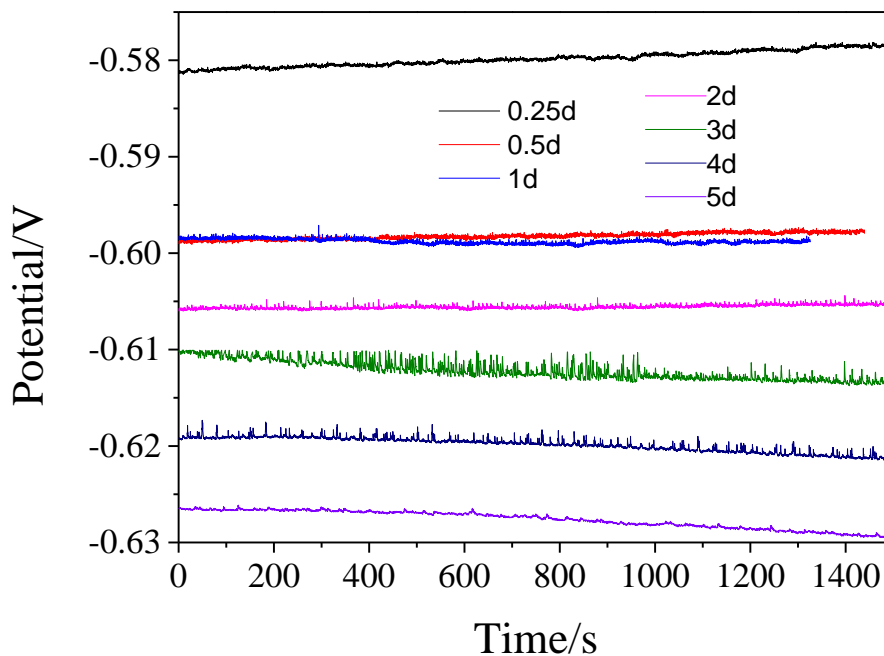


Figure 5. (a) OCP of cast iron in *T.f* system

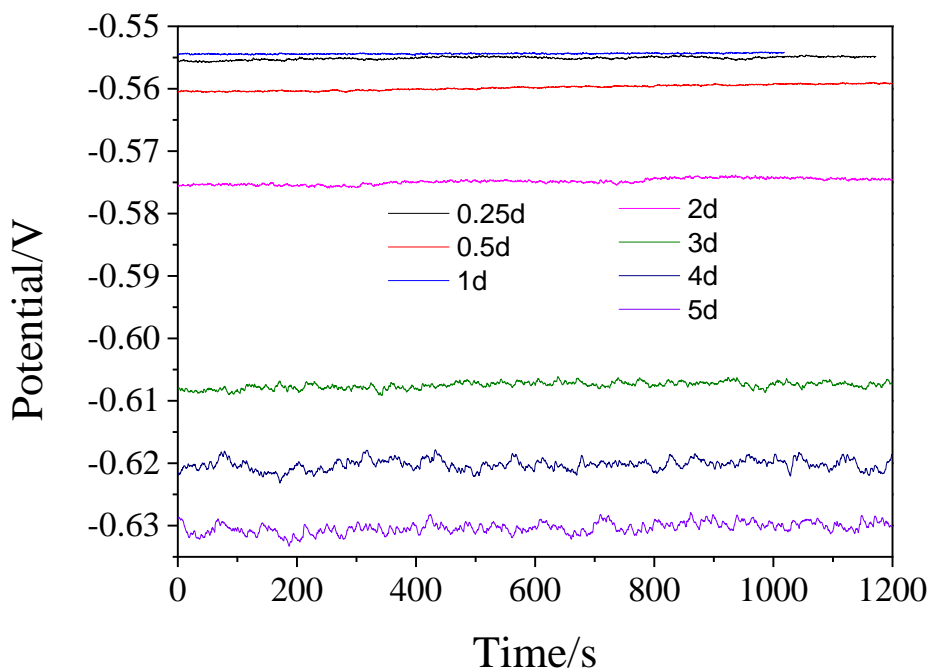


Figure 5. (b) OCP of cast iron in sterile system

In the sterile system, the OCP showed a trend to negative shifts because hydrogen evolution occurred throughout the entire period. The tendency for metal corrosion gradually increased. Fig. 5(a) showed that the OCP significantly shifted in the negative direction during the first 3 days of immersion, and then tended to remain constant for the next two days. The presence of bacteria in the first 3 days may have accelerated corrosion. Over the following two days, the bacteria began to decay,

and both systems then became dominated by hydrogen evolution corrosion at similar rates. This indicated that the bacteria could promote corrosion of cast iron.

### 3.4.2 Electrochemical impedance spectroscopy

Nyquist plots of cast iron in the *T.f* and sterile systems were shown Figs. 6(a) and (b), respectively.

Hydrogen evolution from the cast iron occurred in the acidic medium. The radii of the capacitating arcs increased with time in the *T.f* system as shown in Fig. 6(a).

The radii of the impedance spectra of samples immersed for 6-12 h decreased which could be ascribed to an enhancement in the surface area of the working electrode owing to generation of corrosion pits and the fewer formation of corrosion products on the surface of cast iron during the initial stage of corrosion. *T.f* kept accumulating on the surface of the matrix, causing the corrosion rate to increase. Zhao found that EIS inhibited the growth of bacteria biofilm [36].

According to the principles of chemical equilibrium, as the bacterial strain oxidized  $\text{Fe}^{2+}$  to  $\text{Fe}^{3+}$  to provide energy for its own growth, the anodic reaction  $\text{Fe} - 2e \rightarrow \text{Fe}^{2+}$  continued, and the sample was continuously corroded. The extent of corrosion reached a maximum after 12 h of immersion. However, for immersion of the coupons for periods ranging from 12 h – 5 d, the radii of the impedance spectra increased because corrosion products and extracellular polymeric substance continually accumulated on the surface of the working electrode in this study. Similarly, the EIS of steel A3 in *T.f* system tended to increase with an extension of immersion time [37].

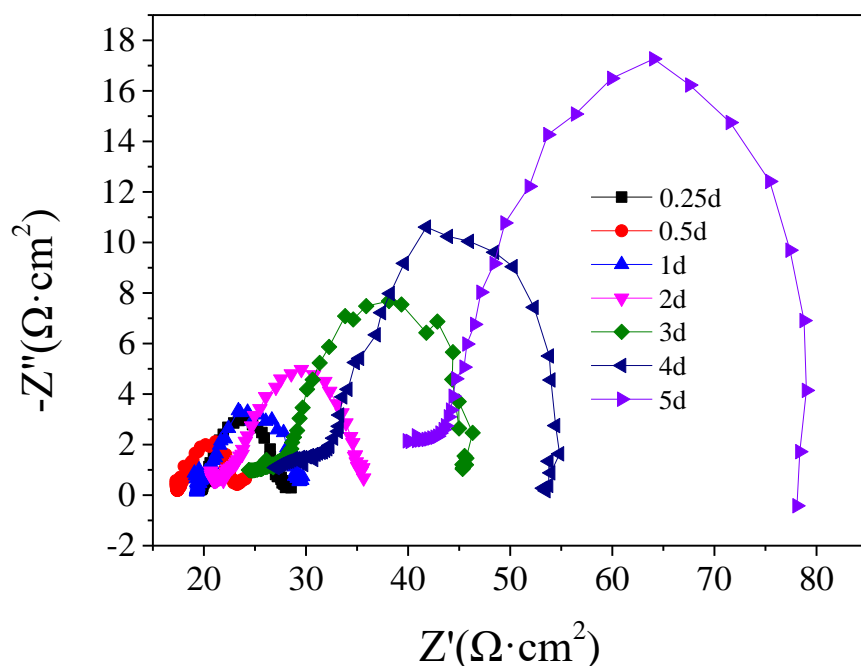


**Figure 6.** (a) EIS of cast iron in *T.f* system

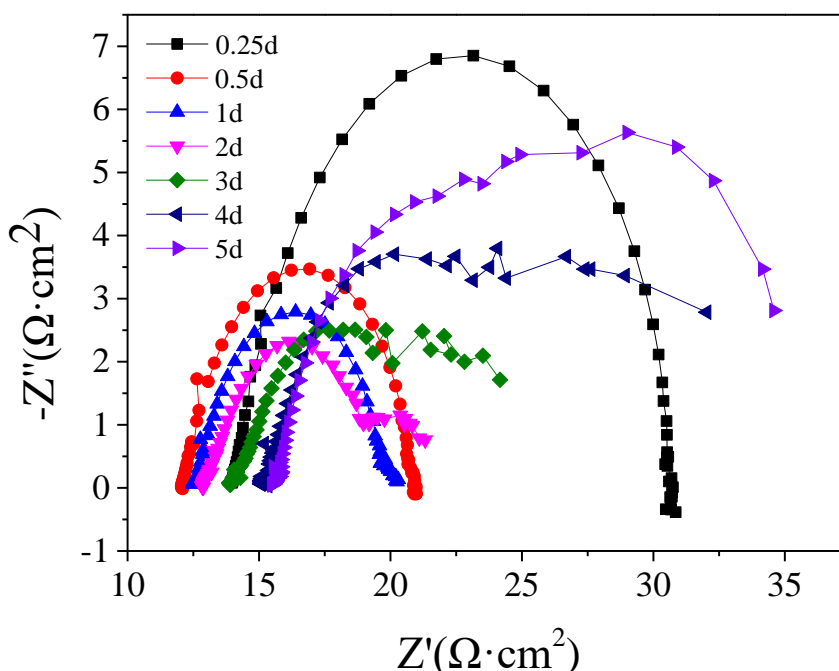


Figure 6. (b) EIS of cast iron in Sterile system

This composite membrane layer, which formed a barrier that protected the matrix of the coupons, became increasingly dense and the capacitive reactance arc modulus enlarged with time, giving rise to a decrease of roughness and a well-distributed electric field at the surface of the working electrodes. Therefore, the corresponding  $R_t$  (charge-transfer resistance) and  $R_b$  (biofilm resistance) increased and the rate of anodic corrosion slowed down, the impedance spectral radius increased, and the corrosion rate of cast iron slowed down.

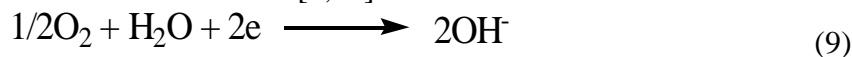
Two anodic reactions occurred in the *T.f* system:



cathodic reaction :



This sequence contradicted that proposed by Liu and Lv, who indicated that oxygen inhalation reactions occurred as followed [6,38] :



The difference may be attributed to the neutral solution pH. Reaction (8) was dominant compared with reaction (9) in the initial phase. In addition, Li found that the biofilm changed the anode and cathode reactions [39]. Owing to the oxidation of *T.f*, reactions (1) and (5) continued in the forward direction, which accelerated dissolution and the corrosion rate of the cast iron. Likewise, electrochemical measurements by Moradi and Duan showed that the corrosion rate of 316 stainless steel increased obviously in the presence of IOB [40]. After two days, *T.f* formed a dense composite film of corrosion products on the electrode surface, which blocked and protected the matrix and slowed down the corrosion.

In the sterile system, the impedance arc first decreased and then increased. In general, the size of the impedance arc was related to the formation of a corrosion product film on the electrode surface. A dense corrosion product film could protect the electrode. When the film had good integrity, the impedance arc was large; if the impedance arc decreased, the film formed was defective or broken.

In these experiments, the measured impedance spectra radii for immersion times of 6 h to 2d gradually decreased, which might result from an increase in contact area between H<sup>+</sup> and the matrix in the solution as the corrosion time and number of surface corrosion pits increased, resulting in an increase in the corrosion rate. Furthermore, the corrosion product film that formed was thin or incomplete, leading to a smaller impedance arc. The measured impedance spectra radii gradually increased after 2 days, which might be due to densification of the corrosion products attached to the surface of the cast iron matrix, which then acted as a barrier and protected the matrix from corrosion; thus, the corrosion rate slowed down as the radii of the impedance spectra increased.

Throughout the entire experimental period, the impedance spectra of cast iron in the two experimental systems took the shape of a half arc, and the radii first decreased and then increased. Moreover, for the same immersion period, the impedance radii of the cast iron electrode in the *T.f* system were smaller than those of the sterile system, which demonstrated that the corrosion trend was larger. This result indicated that *T.f* was beneficial to the corrosion of cast iron, which was consistent with the results of weight loss and morphology observation.

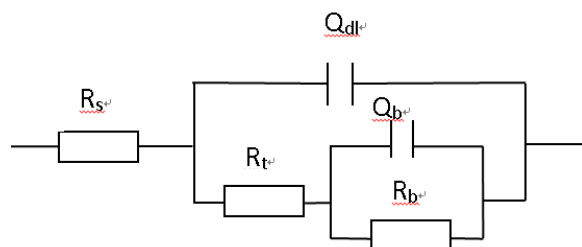


**Figure 7.** Equivalent circuit diagram of EIS

All data for the *T.f* and sterile systems were analyzed using an R(Q(R(QR))) equivalent circuit diagram (Fig. 7), where  $R_s$  represented solution resistance,  $Q_{dl}$  represented double layer capacitance,  $R_t$  represented charge transfer resistance,  $Q_b$  and  $R_b$  represented the capacitance and the resistance of the biofilm or corrosion product film, respectively.

**Table 3** The fitting results of EIS parameters in two systems for different time

	Time	$R_s$	$Q_{dl}$	$R_t$	$Q_b$	$R_b$	Chsq
	(h)	( $\Omega \cdot \text{cm}^2$ )	( $\mu\text{F} \cdot \text{cm}^{-2}$ )	( $\Omega \cdot \text{cm}^2$ )	( $\mu\text{F} \cdot \text{cm}^{-2}$ )	( $\Omega \cdot \text{cm}^2$ )	( $\chi^2$ )
<i>T.f</i>	6h	13.81	0.0116	7.756	0.002472	8.771	1.05E-04
	12h	7.02	0.01135	5.751	5.172	1.436	6.64E-05
	1d	19.18	0.01418	3.452	0.006473	7.022	7.88E-05
	2d	20.53	0.009157	4.03	0.01619	11.42	6.47E-05

	3d	24.74	0.004674	4.67	0.0229	16.66	1.51E-04
	4d	26.42	0.003161	7.254	0.02401	21.3	4.31E-04
	5d	40.73	0.003723	5.374	0.02798	32.14	1.14E-03
sterile	6h	14.05	0.001188	16.46	0.02934	0.2757	1.02E-04
	12h	12.12	0.002554	8.801	0.6943	0.107	3.27E-05
	1d	12.57	0.006387	7.292	9.049	0.3728	4.37E-05
	2d	12.93	0.1075	5.067	0.004278	1.873	6.75E-05
	3d	13.99	0.1078	2.86	0.00931	4.429	1.97E-04
	4d	15.14	0.02952	12.22	0.9735	4.531	2.74E-04
	5d	15.6	0.0241	13.89	0.3377	16.58	4.36E-04

The data in Table 3 showed that  $R_b$  was lowest for the 12 h coupons in the *T.f* system, indicating that the corrosion rate of cast iron was largest for this immersion time. Because bacteria and  $H^+$  attached to the surface of the iron, the generated biofilm was not uniform, which accelerated its corrosion of cast iron.

After 12 h,  $R_b$  continued to grow and the corrosion products on the surface of cast iron gradually increased. Under these conditions, it was not easy for the corrosive medium to contact the surface of the matrix and the corrosion rate decreased.

$R_t$  was used as a standard to evaluate the relative corrosion rates. Comparing the  $R_t$  values for different immersion durations in the sterile system showed that the charge-transfer resistance gradually decreased and corrosion occurred easily from 6 h-3 d, but  $R_t$  increased significantly from 3 to 5 d. This was due to the formation of a thick corrosion product film on the surface, slowing down of the surface electrochemical process, and a corresponding decline in the corrosion rate.

#### 4. CONCLUSIONS

The corrosion behavior of cast iron in the presence of *T.f* was studied. Serious corrosion was detected on cast iron associated with this bacterium and the corrosion rate in the presence of *T.f* was about twice that of acidic water. The results from this study showed that *T.f* bacteria oxidized  $Fe^{2+}$  to  $Fe^{3+}$  when the bacteria used  $Fe^{2+}$  as the energy source and as electron donors, which accelerated corrosion of cast iron. The pH in the *T.f* medium was lower than in the sterile system, which promoted continuation of the corrosion reaction. SEM results demonstrated that the corrosion product film was loose and flawed for coupons immersed in the presence of *T.f*, but more compact and with lamellar products arranged in a dense and orderly manner in local areas for the sterile coupons. When the film was removed, the corrosion pits of the bacteria system were large and deep, and formed in series. Uniform corrosion generation was expected, but pitting was discovered on the cast iron surface in the existence of *T.f*, which could have arisen from localized corrosive surroundings or crevice corrosion owing to attached *T.f* bacteria.

## ACKNOWLEDGMENTS

This project is supported financially by the Opening Project of Key Laboratory of Material Corrosion and Protection of Sichuan Province (No. 2020CL18), the undergraduate innovation and business startups training program of SUSE (No. CX2020012), the Opening Foundation of Sichuan Province Engineering Center for Powder Metallurgy(No. SC-FMYJ2019-07), the Opening Project of Sichuan Province University Key Laboratory of Bridge Non-destruction Detecting and Engineering Computing (No. 2018QYJ03, 2018QZY01).

## References

1. J., M., Byrne, N., Klueglein, C., Pearce, K., M. and Rosso, *Science*, 347 (2015) 1473.
2. J.M. Mcbeth and E. David, *Front. Microbiol.*, 7 (2016) 767.
3. R. Sachan and A.K. Singh, *Anti-corros. Method. M.*, 66 (2019) 19.
4. J. Starosvetsky, R. Kamari, Y. Farber, D. Bilanovic and R. Armon, *Corros. Sci.*, 102 (2016) 446.
5. Yuanyuan, Pan, Xunan, Yang, Meiyang, Xu, Guoping and Sun, *Front. Microbiol.*, 8 (2017) 1.
6. H. Liu, T. Gu, G. Zhang, Y. Cheng, H. Wang and H. Liu, *Corros. Sci.*, 102 (2016) 93.
7. M.A.D.D. Rienzo, M. Aguirre, P.J. Martin and M. Galicia, *Anti-corros. Method. M.*, 65 (2018) 152.
8. F. Xu, Z. Qiu, R. Qiu, J. Yang and C. Lin, *Anti-corros. Method. M.*, 65 (2018) 46.
9. I.M. Zin, V.I. Pokhmurskii, S.A. Korniy, O.V. Karpenko, S.B. Lyon, O.P. Khlopyk and M.B. Tymus, *Anti-corros. Method. M.*, 65 (2018) 517.
10. A.R. Colmer and M.E. Hinkle, *Science*, 106 (1947) 253.
11. M. Nemati, S.T.L. Harrison, G.S. Hansford and C. Webb, *Biochem. Eng. J.*, 1 (1998) 171.
12. R. Jia, D. Yang, D. Xu and T. Gu, *Corros. Sci.*, 145 (2018) 47.
13. R.C. Blake and E.A. Shute, *J. Biol. Chem.*, 262 (1987) 14983.
14. J.C. Cox and D.H. Boxer, *Biotechnol. Appl. Biochem.*, 8 (1986) 269.
15. A. Djebli, P. Proctor, R.C.B. Ii and M. Shoham, *J. Mol. Biol.*, 227 (1992) 581.
16. W.J. Ingledew and A. Houston, *Biotechnol. Appl. Biochem.*, 8 (1986) 242.
17. A.B. Jensen and C. Webb, *Process Biochemistry*, 30 (1995) 225.
18. C. Rai, *Biotechnol. Prog.*, 1 (1985) 200.
19. X. Yang, X. Zhang, Y. Fan and H. Li, *Biochem. Eng. J.*, 42 (2008) 166.
20. A.E. Torma and G.G. Gabra, *Anton. Leeuw. Int. J. G.*, 43 (1977) 1.
21. P. Kaewkannetra, F.J. Garcia-Garcia and T.Y. Chiu, *Int. J. Miner., Metall. Mater.*, 16 (2009) 368.
22. T. Wood, K. Murray and J. Burgess, *Appl. Microbiol. Biotechnol.*, 56 (2001) 560.
23. C. Gómez and K. Bosecker, *Geomicrobiol. J.*, 16 (1999) 233.
24. D. Dierksen, P. Kühner, A. Kappler and K.G. Nickel, *J. Eur. Ceram. Soc.*, 31 (2011) 1177.
25. H. Wang, L.K. Ju, H. Castaneda, G. Cheng and B.M.Z. Newby, *Corros. Sci.*, 89 (2014) 250.
26. C. Pisapia, B. Humbert, M. Chaussidon and C. Mustin, *Geomicrobiol. J.*, 25 (2008) 261.
27. K. Soe, S.M. Li, J.H. Liu and M. Yu, *Acta Phys.-Chim. Sin.*, 24 (2011) 2633.
28. G. F. Xi, X. D. Zhao, S. Wang, J. Yang, J. Sun, Z. Y. An, Y. Li and X. Qu, *Int. J. Electrochem. Sci.*, 15 (2020) 361.
29. D. Xu, Y. Li and T. Gu, *Bioelectrochemistry*, 110(2016) 52.
30. X. Zhao, K. Chen, J. Yang, G. Xi, H. Tian and Q. Chen, *Int. J. Electrochem. Sci.*, 14 (2019) 875.
31. P. Angella and K. Urbanich, *Corros. Sci.*, 42 (2000) 897.
32. S. Feng, H. Yang, Y. Xin, L. Zhang, W. Kang and W. Wang, *J. Ind. Microbiol. Biotechnol.*, 39 (2012) 1625.
33. R. Jia, D. Yang, D. Xu and T. Gu, *Bioelectrochemistry*, 118 (2017) 38.
34. Y. Dong, B. Jiang, D. Xu, C. Jiang, Q. Li and T. Gu, *Bioelectrochemistry*, 123 (2018) 34.
35. S. M. Li, Y. Y. Zhang, J. H. Liu and M. Yu, *Acta Phys. Chim. Sin.*, 24(2008)1553. (in Chinese)

36. Y. Zhao, E. Zhou, Y. Liu, S. Liao, Z. Li, D. Xu, T. Zhang and T. Gu, *Corros. Sci.*, 126 (2017) 142.
37. S. M. Li, Y. Y. Zhang, J. Du, J. H. Liu and M. Yu, *Acta Chim. Sin.*, 68(2010)67. (in Chinese)
38. M. Y. Lv, M. Du, X. Li, Y. Y. Yue and X. C. Chen, *J. Mater. Res. Technol.*, 8(2019)4066.
39. Q. Li, L. Dong, Y. Yang, Z. Wu, H. Zhu, Y. Dong, Y. Shen, L. Zhang and Q. Lu, *Int. J. Electrochem. Sci.*, 15 (2020) 470.
40. M. Moradi, J. Duan, H. Ashassi-Sorkhabi and X. Luan, *Corros. Sci.*, 53 (2011) 4282.

© 2021 The Authors. Published by ESG ([www.electrochemsci.org](http://www.electrochemsci.org)). This article is an open access article distributed under the terms and conditions of the Creative Commons Attribution license (<http://creativecommons.org/licenses/by/4.0/>).